J Neurosurg 119:172–179, 2013
©AANS, 2013

Colocalization of thin-walled dome regions with low hemodynamic wall shear stress in unruptured cerebral aneurysms

Clinical article

Laith M. Kadasi, B.Sc.,[1,2] Walter C. Dent, M.S.,[1] and Adel M. Malek, M.D., Ph.D.[1,2]

[1]Cerebrovascular and Endovascular Division, Department of Neurosurgery, Tufts Medical Center; and [2]Tufts University School of Medicine, Boston, Massachusetts

Object. Wall shear stress (WSS) plays a role in regulating endothelial function and has been suspected in cerebral aneurysm rupture. The aim of this study was to evaluate the spatial relationship between localized thinning of the aneurysm dome and estimated hemodynamic factors, hypothesizing that a low WSS would correlate with aneurysm wall degeneration.

Methods. Steady-state computational fluid dynamics analysis was performed on 16 aneurysms in 14 patients based on rotational angiographic volumes to derive maps of WSS, its spatial gradient (WSSG), and pressure. Local dome thickness was estimated categorically based on tissue translucency from high-resolution intraoperative microscopy findings. Each computational model was oriented to match the corresponding intraoperative view and numerically sampled in thin and normal adjacent dome regions, with controls at the neck and parent vessel. The pressure differential was computed as the difference between aneurysm dome points and the mean neck pressure. Pulsatile time-dependent confirmatory analysis was carried out in 7 patients.

Results. Matched-pair analysis revealed significantly lower levels of WSS (0.381 Pa vs 0.816 Pa; $p < 0.0001$) in thin-walled dome areas than in adjacent baseline thickness regions. Similarly, log WSSG and log WSS × WSSG were both lower in thin regions (both $p < 0.0001$); multivariate logistic regression analysis identified lower WSS and higher pressure differential as independent correlates of lower wall thickness with an area under the curve of 0.80. This relationship was observed in both steady-state and time-dependent pulsatile analyses.

Conclusions. Thin-walled regions of unruptured cerebral aneurysms colocalize with low WSS, suggesting a cellular mechanotransduction link between areas of flow stasis and aneurysm wall thinning.
(http://thejns.org/doi/abs/10.3171/2013.2.JNS12968)

Key Words • **aneurysm** • **hemodynamics** • **shear stress** • **pressure** • **wall thickness** • **intraoperative microscopy** • **vascular disorders**

Cerebral aneurysms represent a significant public health risk and constitute the underlying cause in 85% of SAH cases.[33] Subarachnoid hemorrhage carries a high risk of morbidity and mortality,[16] and preventative surgical and endovascular procedures are associated with nonnegligible age-dependent risks of complication.[28,35] Understanding aneurysm pathogenesis and the patient-specific risk factors associated with rupture would, therefore, be useful in clinical decision making. Several approaches have been considered, including the identification of morphological, histological, and hemodynamic features associated with aneurysm growth and subsequent rupture, with an increasing trend toward the use of CFD in evaluating the role of hemodynamic shear forces on the arterial endothelium.[3,4,13,30,36] These studies have yielded questions regarding the relative importance of regions with high or low flow, and the attendant WSS, in the events leading to aneurysm rupture. Wall shear stress, the frictional force exerted tangentially by the circulating blood on the vessel wall, is particularly important in endothelial gene expression regulation, cellular cytoskeleton organization, and the activation of ion channels.[9,27]

Aneurysm wall thickness is not easily measurable from the image data currently used in many aneurysm visualization protocols, and recent studies on CFD applied patient-specific endoluminal geometries derived from multimodal angiographic images while assuming fixed wall thickness and constant material properties.[3,4,7,14,22,30] However, as a cerebral aneurysm develops, destructive remodeling is thought to occur through spatial disorganization of the endothelium and thinning of the internal elastic lamina and tunica media, with accompanying inflammatory changes, T cell and macrophage infiltration, and the release of lytic enzymes.[1,13,20,24] The net effect of this complex remodeling process is a modification in wall thickness that is readily visible during microsurgical dissection and observation, with thinning regions of the aneurysm dome identified during surgical observation and correlated with the site of rupture.[2,14,15,18,25] These changes provide a rich source of readily quantifiable data that can be used to de-

Abbreviations used in this paper: ACoA = anterior communicating artery; CFD = computational fluid dynamics; MCA = middle cerebral artery; PD = pressure differential; SAH = subarachnoid hemorrhage; WSS = wall shear stress; WSSG = WSS gradient.

Brought to you by Tufts University | Unauthenticated | Downloaded 11/04/25 02:25 PM UTC

scribe systematic intraaneurysmal differences that vary in association with risk factors such as patient sex and aneurysm size.[18] As of yet, there have been no data on the relationship between local hemodynamic variables within the aneurysm dome and direct in vivo observation of aneurysm wall properties in human studies.

The aim of this project is to elucidate the relationship between aneurysm wall thinning and the local prevailing hemodynamics. Specifically, we hypothesize that regions of intraoperatively observable thin translucent tissue colocalize with low WSS. To test this hypothesis, we analyzed visual intraoperative microscopy data corresponding to thin and normal adjacent tissue regions on the aneurysm dome obtained during microsurgical clipping procedures. These images were assessed and correlated with the matched comprehensive CFD analysis based on corresponding 3D high-resolution endoluminal vascular models derived from preoperative catheter-based rotational cerebral angiography.

Methods

Patient Selection

All image data were obtained in patients undergoing microsurgical aneurysm clipping at Tufts Medical Center between November 2006 and May 2011. Sixteen unruptured, saccular, cerebral aneurysms with regions of thin translucent tissue were selected based on simultaneous availability of high-quality intraoperative microscopy video and high-resolution 3D angiographic data of sufficient quality for accurate segmentation, reconstruction, and computational analysis. Thin regions were defined based on color intensity with respect to the parent vessel wall and adjacent thicker nontranslucent dome regions as previously described.[18] Ruptured aneurysms were excluded from the current study because of potential obscuration of the aneurysm dome by subarachnoid blood. The study was performed under approval by the Tufts Institutional Review Board.

Intraoperative Video

All intraoperative images were captured using a Leica M525 OH4 surgical microscope video attachment with a Sony 3-chip CCD (charge-coupled device) color digital video camera at 640 × 480 resolution during aneurysm clipping procedures as recently described.[18] Representative intraoperative photographs of the aneurysm dome were extracted from the video data, and regions of the dome were divided into thin- and thick-walled regions based on color and translucency of the aneurysm dome (Fig. 1). Special care was taken to ensure uniform tissue hydration during region selection. Cases involving light reflection off of the target region were accounted for by assessment from different vantage points during microscope repositioning or by dome movement during dissection.

Computational Fluid Dynamics

Patient-specific aneurysm surface models were constructed from each 3D rotational angiographic volumetric data set using previously developed methods (Fig. 2).[3] Briefly, a tetrahedral mesh was generated from the vascular shell model obtained by threshold segmentation at sufficient cell count to insure mesh density independence. Fluent software (ANSYS, Inc.) was used to solve the Navier-Stokes equations, and Ensight software (CEI Software) was used for postprocessing and sampling. Steady-state analysis was performed under the assumption of a rigid wall with nonslip and nonpenetration in all models. To validate the steady-state results of the study, pulsatile time-dependent CFD analysis (which is computationally time intensive) was performed in a subset of 7 patients using a standardized carotid pulse wave as previously described.[29] To ensure uniformity, the inflow velocity was set to achieve a mean WSS value of 1.5 Pa in the proximal parent vessel at the 5-diameter point distal to the inflow to account for the entrance effect. Computed 3D maps of constant color with underlying WSS, WSSG, and pressure coordinates were oriented to match the intraoperative images prior to comparative analysis (Fig. 3).

Postprocessing and Comparative Analysis

Postprocessing of the CFD data sets was performed using Ensight software (version 9). A total of 80 data points, each containing WSS, WSSG, and pressure values at a given vertex were sampled in a user-blind fashion from each 3D model by a user who was blinded to the CFD results. Each aneurysm contained 20 circumferentially selected points corresponding to baseline healthy tissue sampled from the parent vessel wall, 20 circumferentially selected points corresponding to the aneurysm neck, 20 points corresponding to regions of thin, translucent tissue at the aneurysm dome as determined by user examination of the corresponding intraoperative video data, and 20 points corresponding to baseline thickness areas in the remaining aneurysm sac (Fig. 3A). From these data, derived values of normalized WSS (NormWSS), log WSSG, PD, and log WSS × WSSG product[24] were obtained. Normalized WSS (NormWSS) values at the aneurysm dome were calculated by dividing WSS by the mean parent vessel WSS for that aneurysm. The PD was defined as the difference between each pressure value sampled at a given aneurysm dome and the mean pressure at the aneurysm neck. All statistical analyses, including the matched-pair t-test and multivariate analysis, were performed using JMP (version 8.02, SAS Institute).

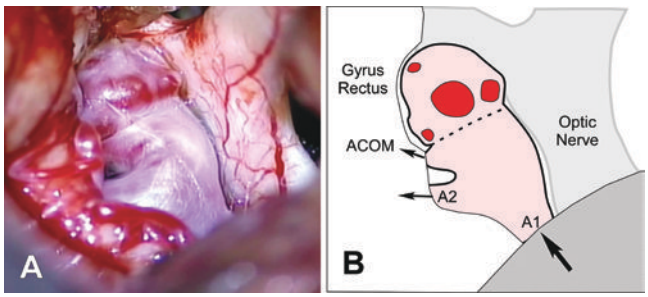


Fig. 1. A: Intraoperative high-resolution microscopic image of an unruptured anterior communicating artery (ACOM) aneurysm from a right frontotemporal approach. **B:** Schematic showing patches of thin, translucent portions of the dome and the aneurysm neck *(dashed line)*.

Brought to you by Tufts University | Unauthenticated | Downloaded 11/04/25 02:25 PM UTC

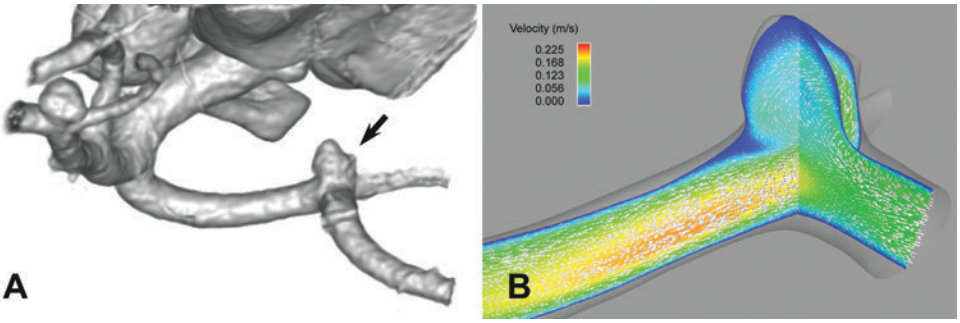


Fig. 2. Case 2. **A:** Volume rendering of a high-resolution 3D rotational angiogram obtained in a patient with an ACoA aneurysm *(arrow)* who underwent a left-sided craniotomy for simultaneous clipping of an MCA aneurysm. **B:** Computational fluid dynamic model of the ACoA aneurysm showing cross-sectional velocity map and vectors.

Evaluation of WSS Ability to Predict Thin-Walled Dome Regions

All 16 aneurysms underwent user-blinded analysis for an assessment of the predictive value of WSS in identifying focal weakness in the aneurysm wall. Using steady-state CFD models illustrating the distribution of WSS, 20 points were selected from regions of the lowest WSS and 20 points from regions of highest WSS. Each of these images was then mapped onto constant color shells illustrating the point location with respect to surrounding aneurysm and vessel geometry. A naive evaluator then reviewed microscopy recordings and labeled each set of constant color points painted above as corresponding to either thick or thin tissue by comparing unlabeled models with the intraoperative appearance of the aneurysm. This was used to obtain a measure of test sensitivity and specificity of WSS as a predictor of aneurysm wall thickness and to evaluate its utility for noninvasive WSS approximation in the assessment of aneurysm wall thickness.

Results

Mean values are presented as the mean ± SEM. Univariate and multivariate analyses of the 16 unruptured saccular aneurysms in 14 patients were carried out with

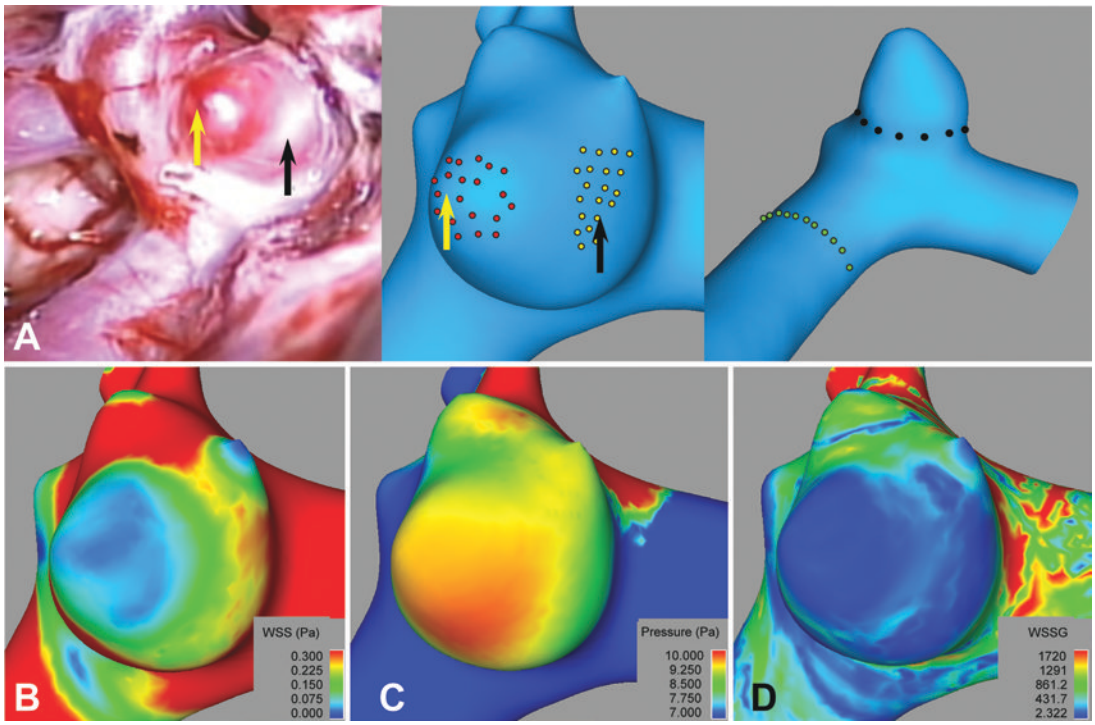


Fig. 3. Illustration of the analysis method. **A:** Intraoperative microscopic image of the aneurysm dome at the time of surgical clipping *(left)* with corresponding sampled regions (*center* and *right*) performed on a constant-color surface representation on the model corresponding to the thin-walled portion of the dome *(yellow arrow)* and adjacent baseline thickness region *(black arrow)*, as well as sampled regions of the parent vessel *(green dots)* and aneurysm neck *(black dots)*. *Red dots* represent manually selected samples corresponding with the thin-walled portion of the aneurysm dome. *Yellow dots* represent manually selected points sampled from the adjacent baseline thickness region of the aneurysm dome. **B–D:** Corresponding computed 3D maps of the WSS (B), pressure (C), and WSSG (D) at which selected sample points from panel A were obtained. Note the expected artifactual microscope light reflection just to the right of the head of the *yellow arrow*.

Brought to you by Tufts University | Unauthenticated | Downloaded 11/04/25 02:25 PM UTC

respect to WSS, WSSG, PD, WSS × WSSG, log WSSG, and log WSS × WSSG. The study group consisted of 2 men and 12 women, with a mean age of 52.1 years (age range 28–69 years; Table 1). The aneurysms used in this study had a mean maximal dome dimension of 4.90 mm and a mean neck size of 3.16 mm. The mean parent vessel WSS across all patients observed via steady-state analysis was 1.52 ± 0.63 Pa.

Thin, Translucent Regions Are Characterized by Lower WSS

Matched-pair analysis was performed at each sampled dome vertex for WSS, PD, and WSSG and was compared between thin translucent and thicker baseline adjacent regions (Fig. 3). The mean WSS was 54% lower in regions of the aneurysm wall corresponding with thin-walled tissue (0.38 ± 0.029 Pa) than at the thicker sampled adjacent aneurysm dome regions (0.82 ± 0.029 Pa; $p < 0.0001$) (Fig. 4 upper). Conversely, the PD with respect to the aneurysm neck was found to be 47% higher at thin-walled regions than at the surrounding aneurysm wall (4.38 ± 0.24 Pa vs 2.98 ± 0.24 Pa; $p < 0.0001$) (Fig. 5 upper) The WSSG ($p = 0.168$) and WSS × WSSG ($p = 0.052$) alone were not statistically significant, potentially due to large magnitude intraaneurysmal differences between the 2 regions, but following logarithmic transformation, both log WSSG ($p < 0.0001$) and log WSS × WSSG ($p < 0.0001$) were found to be significantly lower in thin-walled regions, consistent with colocalization of the latter with regions of relative flow stagnation (Figs. 4 lower and 5 lower).

Logistic Regression Analysis of Thin Regions of the Aneurysm Wall

A stepwise multivariate logistic regression analysis with forward selection was performed on WSS, PD, log WSSG, and log WSS × WSSG with a probability to enter of 0.25 and a probability to leave of 0.1. The only significant independent variables were found to be WSS and PD; these were combined into a multivariate logistic regression model, yielding WSS (OR 1.24 [95% CI 1.17–1.31]; $\chi^2 = 110.3$, $p < 0.0001$) and PD (OR 0.05 [95% CI 0.03–0.09]; $\chi^2 = 61.88$, $p < 0.0001$), with a receiver operating characteristic having an area under the curve of 0.80 for detection of thin translucent tissue.

Time-Dependent Modeling

Confirmatory dynamic time-dependent CFD simulations were performed incorporating pulsatile flow in 7 patients; these stimulations revealed no fundamental difference in the flow pattern between static and dynamic results on the observed relationship between wall thickness and focal hemodynamics. A representative case is shown in Fig. 6 with WSS temporal profile for thin and adjacent normal-thickness dome regions of a distal MCA aneurysm. Time-averaged values of log WSS, log WSSG, and log WSS × WSSG over the entire cardiac cycle were each found to be significantly lower ($p < 0.0001$) in thin-walled regions, consistent with results of the steady-state flow modeling. When averaged over the cardiac cycle, the mean WSS was 69% lower at regions of the aneurysm wall corresponding to thin tissue (0.22 ± 0.03 Pa) than at the surrounding regions of a thicker adjacent aneurysm wall (0.72 ± 0.03 Pa). These differences in WSS between aneurysm dome tissue thickness were also confirmed at peak systolic (thin: 0.33 ± 0.19 Pa vs thick: 0.94 ± 0.19 Pa, $p = 0.0192$) and end diastolic (thin: 0.16 ± 0.09 Pa vs thick: 0.52 ± 0.09 Pa, $p = 0.0079$) time points via matched-pair analysis.

Assessment of Low WSS as a Predictor of Translucent Thin-Walled Regions by Blinded Analysis

To further evaluate the converse predictive utility of low WSS in correlating with thin-walled tissue, additional blinded analysis was performed on each of the 16 an-

TABLE 1: Patient demographics, aneurysm location, and size

Case No.	Age (yrs), Sex	Aneurysm Location	Max Dome Size (mm)	Neck Diameter (mm)
1	63, F	MCA	5.89	4.75
2	47, F	ACoA	2.33	2.42
		MCA	3.51	1.95
3	46, F	MCA	5.03	2.97
4	62, F	MCA	6.28	3.67
5	68, F	MCA	7.37	4.68
6	33, F	ACoA	3.28	2.22
7	69, F	MCA	8.36	3.38
8	54, F	MCA	3.54	2.77
9	43, M	MCA	2.55	2.14
10	50, F	MCA	6.38	3.88
11	57, F	ACoA	4.65	3.57
12	61, F	MCA	3.15	1.33
13	28, M	ACoA	3.43	2.01
14	49, F	MCA	10.13	5.82
		MCA	2.67	3.06

Brought to you by Tufts University | Unauthenticated | Downloaded 11/04/25 02:25 PM UTC

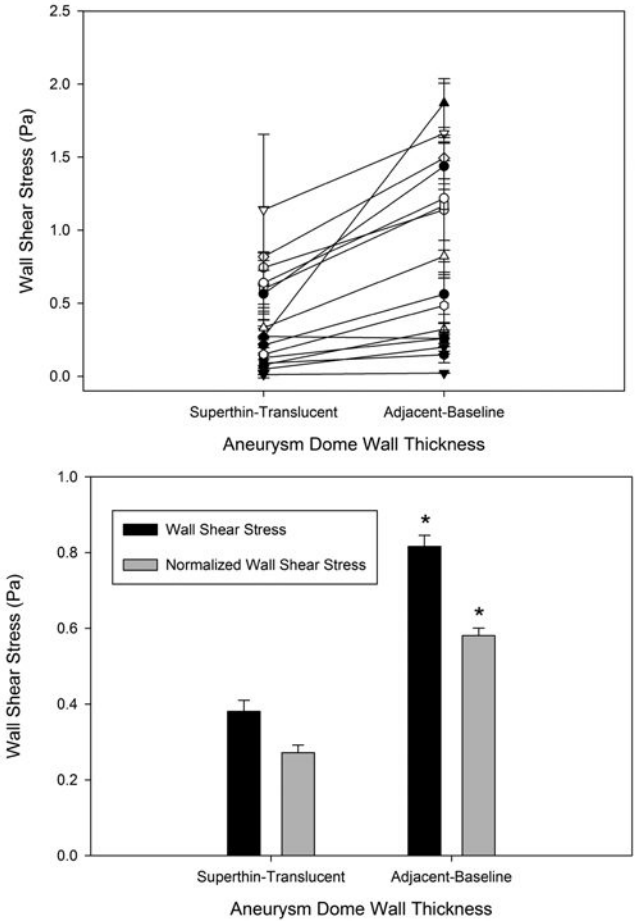


Fig. 4. Upper: Graph comparing on a per-aneurysm basis the WSS in thin- and thick-walled regions of the aneurysm dome. **Lower:** Bar graph showing the mean WSS and mean WSS normalized with respect to the mean parent vessel WSS in all regions based on regional type. *p < 0.0001.

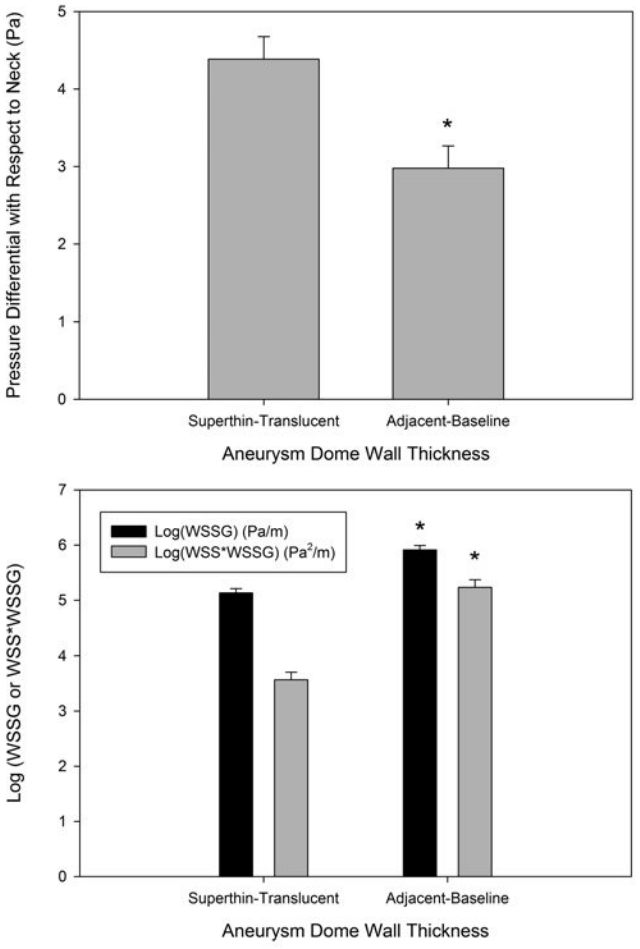


Fig. 5. Upper: Pressure differential between the dome region and mean pressure at the aneurysm neck. **Lower:** Logarithmic transformations of WSSG and WSS × WSSG product reveal lower values in thin-walled regions consistent with flow stasis. *p < 0.0001.

eurysms included in this study. The assumption was made that low WSS would be associated with thin-walled tissue. A naive observer blinded to the CFD results and actual WSS maps was then provided with paired constant-color 3D models of the aneurysm geometry labeled only by points corresponding to high and low WSS regions (preselected based on the CFD results) along with the intraoperative microscopy images. When asked to assign the regions to low or high WSS based on the corresponding intraoperative tissue characteristics from images corresponding to the highlighted vertices on the constant-color 3D models, the observer correctly identified 13 of 16 patients with the corresponding CFD estimate of high versus low WSS. This corresponds to a test sensitivity of 81%, indicating a potential application of WSS maps based on 3D angiography models as a noninvasive predictor of underlying aneurysm dome wall tissue structure.

Discussion

A relationship appears to exist between aneurysm wall thickness and prevailing hemodynamic conditions, particularly WSS. Among the saccular aneurysms in this study, low WSS and high pressure were independently found to colocalize with thin, easily visualized translucent regions of the aneurysm sac. This finding is the first to demonstrate an association between the in vivo appearance of focal degenerative thinning and local mechanical forces in naturally occurring human unruptured cerebral aneurysms.

High Versus Low WSS

The local hemodynamic microenvironment and its influence on the pathophysiology of cerebral aneurysms has been examined at length and is being increasingly considered an important candidate feature in the prediction of aneurysm prognosis. Nonetheless, there remain conflicting data with respect to the relative importance of high versus low WSS in aneurysm rupture. Chronic high WSS has been shown to induce luminal expansion and adaptive arterial remodeling in rodent experiments.[32] In other animal and in vitro studies, high focal hemodynamic WSS and high positive WSSG with direct flow patterns have been associated with endothelial cell depletion, migration away from the high WSS area, and molecular changes in endothelial nitric oxide synthase expression,[24,31,34] with prolonged high WSS potentially contributing to fragmentation of the ves-

Brought to you by Tufts University | Unauthenticated | Downloaded 11/04/25 02:25 PM UTC

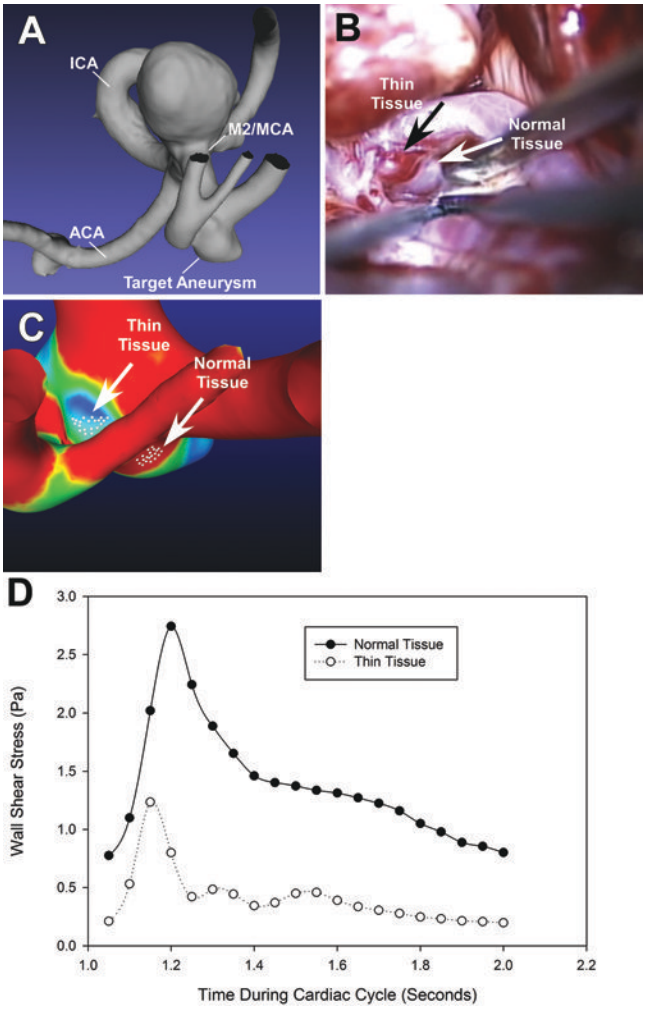


Fig. 6. Case 14. **A:** Volume rendering of a high-resolution 3D rotational angiogram illustrating the location of an MCA aneurysm assessed via confirmatory pulsatile analysis. **B:** Intraoperative microscopic image of the aneurysm dome at the time of surgical clipping indicating foci of thin tissue *(black arrow)* and normal baseline tissue *(white arrow)*. **C:** Corresponding 3D map of computed WSS with the distribution of selected points that were recorded throughout the cardiac cycle. **D:** Mean WSS values of each sample group throughout the cardiac cycle. ACA = anterior cerebral artery; ICA = internal carotid artery.

sel internal elastic lamina as a proposed mechanism of aneurysm initiation.[19] Computational fluid dynamics studies of human vasculature have also supported a role for high WSS and elevated maximum WSS in the rupture of cerebral aneurysms.[5,6,14] In a large CFD examination of qualitative hemodynamic characteristics, concentrated, rapid-flow patterns consistent with high WSS were correlated with aneurysm rupture.[7] Increased hemodynamic forces due to smaller vessel diameter and increased flow velocity have also been associated with the higher incidence of SAH in females over males, which parallels statistically significant sex differences in intraoperatively observed wall thickness distributions at the aneurysm dome.[18,22]

In contrast, low-flow environments and low focal WSS have been theorized to contribute to wall degradation through a static deleterious endothelial phenotype,[11,23] marked by the increased activation of monocytes and platelets, vasoconstriction, paracrine growth stimulation, and an increased oxidant state with endothelial apoptosis and cell turnover.[8,10,12,21] Low WSS at the aneurysm dome has been correlated with wall displacement and aneurysm growth,[4] as well as rupture in MCA and ICA aneurysms.[17,30] Through CFD analysis, low mean WSS over the aneurysm dome has also been identified as an independently significant factor in discriminating rupture status,[36] and ruptured aneurysms were found to have greater aneurysm areas under low WSS and higher percentages of total aneurysm area under low WSS than unruptured aneurysms.[17] Interestingly, low-flow environments in CFD analysis have been repeatedly found to be below the levels associated with flow-mediated expression of endothelin-1 and endothelial nitric oxide synthase in ruptured aneurysms, which has been noted at values less than 0.4 Pa.[3,23,36] The current study indicates the presence of low WSS at sites of clear degenerative changes in the aneurysm wall and suggests that further characterization of the relationship between alterations in wall thickness and flow-mediated gene expression may improve understanding of aneurysm progression toward rupture.

Pressure at Thin-Walled Regions

The intraaneurysmal difference in pressure observed during steady-state modeling in this study between thin- and thick-walled regions of the aneurysm dome was relatively small at 1.4 Pa. However, the colocalization of this focal higher pressure with the translucent thinner regions of the aneurysm wall suggest potentially elevated wall tension, which is approximately inversely proportional to wall thickness and proportional to transmural pressure. As noted, the current study operates under the assumption of a rigid vessel wall. Future fluid-structure analysis incorporating estimated viscoelastic vessel wall properties coupled with computational fluid analysis is needed to further evaluate focal wall tension.

Test Sensitivity

During primary user-blinded evaluations, the use of WSS as a pure predictor of the wall thickness status at a given locus was found to yield a sensitivity of 81%. Although this relationship was correctly identified in 13 of the 16 patients studied, divergence in the remaining cases may be explained primarily by errors in model orientation as well as the presence of diffuse foci of confounding calcification that may contribute to wall thickness by a secondary mechanism. Exploration of a calcification-specific model of aneurysm growth and degeneration may merit further study.

Measurement of Wall Thickness

Wall thickness is a metric that is frequently assessed in the study of vessel wall pathogenesis. Measurement of vessel wall thickness in cerebral aneurysms, however, provides a unique challenge that has been addressed through postexcisional measurement as well as in vivo intraoperative examination.[13,18] Currently, there is no established noninvasive method of directly assessing intra-

Brought to you by Tufts University | Unauthenticated | Downloaded 11/04/25 02:25 PM UTC

cranial aneurysm wall thickness. Although intravascular ultrasonography may serve as a potential approach, there are not yet sufficient data to support the increased risk of intracranial navigation of a sampling microwire with its attendant risk of dissection, thromboembolism, or aneurysm rupture. Recent approaches to noninvasive measurement have included the use of electrocardiographically gated CT angiography to detect pulsation at the aneurysm wall as an approximation of the thinnest regions of the aneurysm dome.[15] In the current study, albeit limited to unruptured aneurysms, high-magnification intraoperative examination failed to show any visible pulsation at thin regions of the aneurysm wall. The availability of a noninvasive methodology for accurate aneurysm wall thickness measurement would enable future studies on the clinical assessment of its link to aneurysm rupture risk.

Study Limitations

Only a small number of cases were examined, which were limited to unruptured aneurysms located at the MCA or ACoA in the anterior circulation. As a result, the observations described in this study may not apply to ruptured cerebral aneurysms or aneurysms found in the posterior circulation. As an inherent limitation of intracranial aneurysm surgery for clipping, intraoperative microscopy did not allow circumferential visualization of the entire aneurysm dome in all cases, although at least 180° visualization of the aneurysm dome was obtained for each patient in the study. Although it is implied that thin-walled regions of the aneurysm dome are more likely to be prone to rupture and SAH, it is possible that the latter occurs in an unrelated region. While extensive experience of surgical exploration of a ruptured aneurysm would suggest otherwise, an explicit link between the thinnest regions of the aneurysm wall and the actual ultimate focus of rupture cannot be inferred from the current study. In addition, as noted in *Methods,* the WSS distributions in this study were obtained via modeling under the assumption of a rigid vessel wall and population-based flow parameters and thus serve only as an approximation of the underlying hemodynamics.

The aneurysms used in this study had a mean maximal dome of 4.90 mm, which is considered small, especially in light of the low rate of only 0.7% per year rupture rate found in the International Study of Unruptured Intracranial Aneurysms (ISUIA) of asymptomatic unruptured lesions smaller than 7 mm.[35] On the other hand, aneurysms smaller than 5 mm are often encountered in clinical practice and comprise greater than 50% of ruptured aneurysms enrolled in the International Subarachnoid Aneurysm Trial (ISAT).[26] Although one can argue that this represents the effect of bias and that ruptured lesions may represent an inflammatory process that is distinct from the pathogenesis of asymptomatic lesions, the study of small aneurysms can potentially yield important data for the understanding of aneurysm development and pathophysiology.

Multiple Mechanisms

The study was limited to the most common classified subset of unruptured aneurysms, those containing regions of thin, translucent tissue, due to the ease with which differences in intraaneurysmal wall thickness may be observed, as well as a suspected divergence in aneurysm pathogenesis from entirely thin-walled sacs as seen in blister aneurysms and aneurysms with thick-walled fibrotic lesions. Differences in the distribution of wall thickness and the presence of thick, calcified tissue at the aneurysm dome may consequently alter the relative importance of the underlying WSS and pressure, and act as a confounder in the use of hemodynamic measures as a determinant of rupture risk in CFD analyses for which wall thickness is not considered.

Conclusions

The results of the current study suggest a possible unifying mechanism for aneurysm progression to rupture, whereby low WSS is associated with thinning of the wall leading to a theoretical increased wall tension in these thin regions of the aneurysm wall. This is the first in vivo study in humans linking the local microhemodynamic environment of cerebral aneurysms estimated by CFD with local variations to aneurysm wall thickness. The uncovered strong relationship between WSS and changes in intracranial aneurysm wall thickness suggest a new avenue for future investigation.

Disclosure

This work was supported by NIH-R21HL102685. L.M.K. was supported by a grant from the Harold Williams Foundation. A.M.M. has received unrestricted research support from Codman Neurovascular, Inc., Stryker Neurovascular, Inc., Microvention-Terumo, Inc., Ansys, Inc., CD-adapco, Inc., and Siemens Medical Imaging for research that is unrelated to this work.

Author contributions to the study and manuscript preparation include the following. Conception and design: Malek. Acquisition of data: Kadasi, Dent. Analysis and interpretation of data: Malek, Kadasi. Drafting the article: Malek, Kadasi. Critically revising the article: all authors. Reviewed submitted version of manuscript: all authors. Approved the final version of the manuscript on behalf of all authors: Malek. Statistical analysis: Malek, Kadasi. Administrative/technical/material support: Dent. Study supervision: Malek.

Acknowledgment

The authors thank Alex Lauric, Ph.D., for her assistance.

References

1. Abruzzo T, Shengelaia GG, Dawson RC III, Owens DS, Cawley CM, Gravanis MB: Histologic and morphologic comparison of experimental aneurysms with human intracranial aneurysms. **AJNR Am J Neuroradiol 19:**1309–1314, 1998
2. Asari S, Ohmoto T: Growth and rupture of unruptured cerebral aneurysms based on the intraoperative appearance. **Acta Med Okayama 48:**257–262, 1994
3. Baharoglu MI, Schirmer CM, Hoit DA, Gao BL, Malek AM: Aneurysm inflow-angle as a discriminant for rupture in sidewall cerebral aneurysms: morphometric and computational fluid dynamic analysis. **Stroke 41:**1423–1430, 2010
4. Boussel L, Rayz V, McCulloch C, Martin A, Acevedo-Bolton G, Lawton M, et al: Aneurysm growth occurs at region of low wall shear stress: patient-specific correlation of hemodynamics and growth in a longitudinal study. **Stroke 39:**2997–3002, 2008

Brought to you by Tufts University | Unauthenticated | Downloaded 11/04/25 02:25 PM UTC

5. Castro MA, Putman CM, Sheridan MJ, Cebral JR: Hemodynamic patterns of anterior communicating artery aneurysms: a possible association with rupture. **AJNR Am J Neuroradiol 30:**297–302, 2009
6. Cebral JR, Castro MA, Burgess JE, Pergolizzi RS, Sheridan MJ, Putman CM: Characterization of cerebral aneurysms for assessing risk of rupture by using patient-specific computational hemodynamics models. **AJNR Am J Neuroradiol 26:** 2550–2559, 2005
7. Cebral JR, Mut F, Weir J, Putman CM: Association of hemodynamic characteristics and cerebral aneurysm rupture. **AJNR Am J Neuroradiol 32:**264–270, 2011
8. Chappell DC, Varner SE, Nerem RM, Medford RM, Alexander RW: Oscillatory shear stress stimulates adhesion molecule expression in cultured human endothelium. **Circ Res 82:**532–539, 1998
9. Chien S: Mechanotransduction and endothelial cell homeostasis: the wisdom of the cell. **Am J Physiol Heart Circ Physiol 292:**H1209–H1224, 2007
10. Cho A, Mitchell L, Koopmans D, Langille BL: Effects of changes in blood flow rate on cell death and cell proliferation in carotid arteries of immature rabbits. **Circ Res 81:**328–337, 1997
11. Dai G, Kaazempur-Mofrad MR, Natarajan S, Zhang Y, Vaughn S, Blackman BR, et al: Distinct endothelial phenotypes evoked by arterial waveforms derived from atherosclerosis-susceptible and -resistant regions of human vasculature. **Proc Natl Acad Sci U S A 101:**14871–14876, 2004
12. De Keulenaer GW, Chappell DC, Ishizaka N, Nerem RM, Alexander RW, Griendling KK: Oscillatory and steady laminar shear stress differentially affect human endothelial redox state: role of a superoxide-producing NADH oxidase. **Circ Res 82:**1094–1101, 1998
13. Frösen J, Piippo A, Paetau A, Kangasniemi M, Niemelä M, Hernesniemi J, et al: Remodeling of saccular cerebral artery aneurysm wall is associated with rupture: histological analysis of 24 unruptured and 42 ruptured cases. **Stroke 35:**2287–2293, 2004
14. Hassan T, Timofeev EV, Saito T, Shimizu H, Ezura M, Matsumoto Y, et al: A proposed parent vessel geometry-based categorization of saccular intracranial aneurysms: computational flow dynamics analysis of the risk factors for lesion rupture. **J Neurosurg 103:**662–680, 2005
15. Hayakawa M, Katada K, Anno H, Imizu S, Hayashi J, Irie K, et al: CT angiography with electrocardiographically gated reconstruction for visualizing pulsation of intracranial aneurysms: identification of aneurysmal protuberance presumably associated with wall thinning. **AJNR Am J Neuroradiol 26:**1366–1369, 2005
16. Hop JW, Rinkel GJE, Algra A, van Gijn J: Case-fatality rates and functional outcome after subarachnoid hemorrhage: a systematic review. **Stroke 28:**660–664, 1997
17. Jou LD, Lee DH, Morsi H, Mawad ME: Wall shear stress on ruptured and unruptured intracranial aneurysms at the internal carotid artery. **AJNR Am J Neuroradiol 29:**1761–1767, 2008
18. Kadasi LM, Dent WC, Malek AM: Cerebral aneurysm wall thickness analysis using intraoperative microscopy: effect of size and gender on thin translucent regions. **J Neurointervent Surg** [epub ahead of print], 2012
19. Kolega J, Gao L, Mandelbaum M, Mocco J, Siddiqui AH, Natarajan SK, et al: Cellular and molecular responses of the basilar terminus to hemodynamics during intracranial aneurysm initiation in a rabbit model. **J Vasc Res 48:**429–442, 2011
20. Kondo S, Hashimoto N, Kikuchi H, Hazama F, Nagata I, Kataoka H: Apoptosis of medial smooth muscle cells in the development of saccular cerebral aneurysms in rats. **Stroke 29:**181–189, 1998
21. Kraiss LW, Geary RL, Mattsson EJR, Vergel S, Au YPT, Clowes AW: Acute reductions in blood flow and shear stress induce platelet-derived growth factor-A expression in baboon prosthetic grafts. **Circ Res 79:**45–53, 1996
22. Lindekleiv HM, Valen-Sendstad K, Morgan MK, Mardal KA, Faulder K, Magnus JH, et al: Sex differences in intracranial arterial bifurcations. **Gend Med 7:**149–155, 2010
23. Malek AM, Alper SL, Izumo S: Hemodynamic shear stress and its role in atherosclerosis. **JAMA 282:**2035–2042, 1999
24. Meng H, Wang Z, Hoi Y, Gao L, Metaxa E, Swartz DD, et al: Complex hemodynamics at the apex of an arterial bifurcation induces vascular remodeling resembling cerebral aneurysm initiation. **Stroke 38:**1924–1931, 2007
25. Mizoi K, Yoshimoto T, Nagamine Y: Types of unruptured cerebral aneurysms reviewed from operation video-recordings. **Acta Neurochir (Wien) 138:**965–969, 1996
26. Molyneux AJ, Kerr RSC, Yu LM, Clarke M, Sneade M, Yarnold JA, et al: International subarachnoid aneurysm trial (ISAT) of neurosurgical clipping versus endovascular coiling in 2143 patients with ruptured intracranial aneurysms: a randomised comparison of effects on survival, dependency, seizures, rebleeding, subgroups, and aneurysm occlusion. **Lancet 366:**809–817, 2005
27. Nixon AM, Gunel M, Sumpio BE: The critical role of hemodynamics in the development of cerebral vascular disease. A review. **J Neurosurg 112:**1240–1253, 2010
28. Raaymakers TWM, Rinkel GJE, Limburg M, Algra A: Mortality and morbidity of surgery for unruptured intracranial aneurysms: a meta-analysis. **Stroke 29:**1531–1538, 1998
29. Schirmer CM, Malek AM: Prediction of complex flow patterns in intracranial atherosclerotic disease using computational fluid dynamics. **Neurosurgery 61:**842–852, 2007
30. Shojima M, Oshima M, Takagi K, Torii R, Hayakawa M, Katada K, et al: Magnitude and role of wall shear stress on cerebral aneurysm: computational fluid dynamic study of 20 middle cerebral artery aneurysms. **Stroke 35:**2500–2505, 2004
31. Tardy Y, Resnick N, Nagel T, Gimbrone MA Jr, Dewey CF Jr: Shear stress gradients remodel endothelial monolayers in vitro via a cell proliferation-migration-loss cycle. **Arterioscler Thromb Vasc Biol 17:**3102–3106, 1997
32. Tuttle JL, Nachreiner RD, Bhuller AS, Condict KW, Connors BA, Herring BP, et al: Shear level influences resistance artery remodeling: wall dimensions, cell density, and eNOS expression. **Am J Physiol Heart Circ Physiol 281:**H1380–H1389, 2001
33. van Gijn J, Rinkel GJE: Subarachnoid haemorrhage: diagnosis, causes and management. **Brain 124:**249–278, 2001
34. Wang Z, Kolega J, Hoi Y, Gao L, Swartz DD, Levy EI, et al: Molecular alterations associated with aneurysmal remodeling are localized in the high hemodynamic stress region of a created carotid bifurcation. **Neurosurgery 65:**169–178, 2009
35. Wiebers DO, Whisnant JP, Huston J III, Meissner I, Brown RD Jr, Piepgras DG, et al: Unruptured intracranial aneurysms: natural history, clinical outcome, and risks of surgical and endovascular treatment. **Lancet 362:**103–110, 2003
36. Xiang J, Natarajan SK, Tremmel M, Ma D, Mocco J, Hopkins LN, et al: Hemodynamic-morphologic discriminants for intracranial aneurysm rupture. **Stroke 42:**144–152, 2011

Manuscript submitted June 3, 2012.
Accepted February 7, 2013.
Please include this information when citing this paper: published online March 29, 2013; DOI: 10.3171/2013.2.JNS12968.

Address correspondence to: Adel M. Malek, M.D., Ph.D., Department of Neurosurgery, Tufts Medical Center, 800 Washington Street, Boston, Massachusetts 02111. email: amalek@tuftsmedicalcenter.org.

Brought to you by Tufts University | Unauthenticated | Downloaded 11/04/25 02:25 PM UTC